

Identifying the magnetic genes in fully- and partially-ordered V_2XAl ($X = Cr, Mn, Fe, Co, Ni$) Heusler alloys

Zhenyang Xie,¹ Yuntao Wu,¹ Jitong Song,¹ Yuanji Xu,^{1,*} and Fuyang Tian^{1,†}

¹*Institute for Applied Physics and Department of Physics,
University of Science and Technology Beijing, Beijing 100083, China*

(Dated: August 26, 2025)

Multicomponent Heusler alloys exhibit various magnetic properties arising from their diverse atomic compositions and crystal structures. Identifying the general physical principles that govern these behaviors is essential for advancing their potential in spintronic applications. In this work, we combine density functional theory with atomistic Monte Carlo simulations to investigate the magnetic ground states, finite-temperature magnetic transitions, and electronic structures of fully-ordered $L2_1$ -, XA -type, and partially-ordered V_2XAl ($X = Cr, Mn, Fe, Co, Ni$) Heusler alloys. We introduce the concept of magnetic genes, defined as $V-X-V$ triangular motifs connected by the nearest-neighbor (NN) exchange interactions J_{V-X} . Within this framework, the magnetic ground states and transition temperatures across the V_2XAl family can be consistently understood. The magnetic order is primarily governed by the NN J_{V-X} interactions in the triangular genes, while the transition temperatures are additionally influenced by J_{X-X} couplings. Furthermore, the magnetic genes are still proven to be effective in our calculations on partially-ordered V_2XAl alloys from $L2_1$ to XA -type structures. Our results suggest that the concept of magnetic genes provides a unifying principle for understanding magnetic ordering in V -based Heusler alloys and could serve as a powerful guide for exploring magnetism and designing advanced spintronic materials in a broader class of Heusler systems.

I. INTRODUCTION

Heusler alloys, long regarded as prototypical spintronic materials owing to their half-metallic nature, are capable of delivering nearly 100% spin polarization at and even well above room temperature [1–6]. Consequently, the discovery and design of high-performance Heusler compounds remain a central objective of both experimental and theoretical research [7]. On the experimental side, typical full-Heusler alloys such as Co_2CrAl and Co_2TiSn have been shown to sustain ferromagnetic order up to room temperature, with Curie temperatures T_C of approximately 335 K and 333 K, respectively [8, 9]. Over the past two decades, theoretical efforts, particularly high-throughput first-principles calculations combined with Monte Carlo or spin-model simulations, have identified dozens of full-Heusler systems exhibiting magnetic anisotropy energies exceeding 1 MJ/m^3 together with Curie temperatures above 500 K [10, 11]. These advances have substantially expanded the library of high-performance magnets and promising high- T_C candidates for spintronic applications [12].

In particular, full-Heusler alloys with the general formula X_2YZ ($Y =$ transition metals) have attracted considerable attention owing to their rich magnetic properties, shape-memory behavior, and sensitivity to chemical disorder [13–15]. For instance, Co_2VAl exhibits ferromagnetic ordering with a Curie temperature close to room temperature, while its T_C decreases under applied external pressure [16]. In contrast, Mn_2VGa shows

ferrimagnetic ordering with a significantly higher Curie temperature of 784 K [17]. The inverse-Heusler (XA -type) compound Mn_2CoAl also displays robust ferromagnetism, with a T_C of 720 K at ambient pressure [18], whereas Mn_2FeSi , despite sharing the same crystal structure, has an anomalously low T_C of only 67 K [19]. Moreover, both theoretical and experimental studies of $L2_1$ -type full-Heusler alloys have revealed complex magnetic behavior. For example, Co_2FeSi exhibits a remarkably high Curie temperature of about 1100 K [20], while Fe_2VAl remains paramagnetic up to room temperature. Such diverse magnetic orders are generally attributed to variations in stoichiometry and chemical disorder [21], raising fundamental questions about the key factors that govern the magnetic properties of Heusler systems.

Recently, chemical disorder has attracted growing attention as an effective means of tuning magnetic order. Disorder can substantially modify magnetic exchange interactions, influence phase stability, and reshape the overall magnetic state of a material [22–24]. For example, studies on Ru_2MnZ ($Z = Sn, Sb, Ge, Si$) full-Heusler alloys have demonstrated the strong impact of chemical disorder on their magnetic behavior [22], with Co_2FeSn exhibiting enhanced magnetism and pronounced size-dependent disorder effects [25]. Similarly, Smith *et al.* recently employed DC magnetron sputtering to grow epitaxial V_2FeAl thin films [26]. Although V_2FeAl shows a relatively high Curie temperature experimentally, its crystal structure appears to be a mixture of the XA - and $L2_1$ -type phases, complicated further by intrinsic disorder [26]. Other works have demonstrated that increasing the degree of chemical disorder leads to a pronounced suppression of spontaneous magnetization and Curie temperature [26, 27]. From a broader phys-

* yuanjixu@ustb.edu.cn

† fuyang@ustb.edu.cn

ical perspective, the deliberate introduction of chemical disorder not only provides an alternative strategy for tuning magnetism but also establishes a promising platform to investigate the fundamental mechanisms underlying complex magnetic orders in Heusler alloys [24].

Although the magnetic properties of full-Heusler alloys have been extensively investigated experimentally, the underlying mechanisms remain elusive due to their complex atomic compositions, multi-sublattice character, and the presence of chemical disorder. Using first-principles approaches, previous works have systematically evaluated the magnetic exchange couplings J_{ij} for several Heusler alloy families employing frozen-magnon and linear-response techniques [28, 29]. For vanadium-based antiferromagnets, existing studies have primarily concentrated on the ordered $L2_1$ -type structure of V_2YAl ($Y = Nb, Ta$) [30]. Follow-up investigations extended this work by comparing the $L2_1$ phase with the inverse XA phase across a broader range of compounds. In particular, Kuroda *et al.* reported that $L2_1$ -type V_2NbAl and V_2TaAl favor antiferromagnetic coupling, whereas in V_2YSi ($Y = Ti, Zr, Hf$), the XA structure often competes with or destabilizes the $L2_1$ phase [30]. In addition, large-scale first-principles screenings of the inverse-Heusler X_2YZ chemical space, where $X = Sc, Ti, V, Cr, Mn$; $Z = Al, Si, As$; and Y spans from Ti to Zn , have identified the necessary conditions for the emergence of semimetallic states and established three Slater–Pauling rules associated with d - d hybridization [31]. Despite these advances, the systematic experimental synthesis and theoretical calculations of V-based V_2XAl compounds with the complete set of $X = Cr, Mn, Fe, Co$, and Ni are still lacking. A comprehensive microscopic understanding of the mechanisms that govern magnetism in both fully- and partially-ordered V-based full-Heusler alloys is therefore essential.

In this work, we investigate the ground-state magnetic orders and electronic structures of V_2XAl ($X = Cr, Mn, Fe, Co, Ni$) Heusler alloys using density functional theory. For the fully-ordered $L2_1$ -type V_2XAl , V_2CrAl and V_2MnAl exhibit ferrimagnetic order, whereas the remaining compounds adopt ferromagnetic order. The situation becomes more intricate in the inverse XA -type V_2XAl . While V_2CrAl displays a nearly vanishing net magnetic moment with ferromagnetic order between the two different Wyckoff sites of V atoms, the other four alloys exhibit ferrimagnetic order with antiparallel spin alignment between the two V sublattices. Despite this diversity, the magnetic orders across V_2XAl compounds can be consistently interpreted in terms of the V- X -V triangular pathway, governed by the NN magnetic exchange coupling J_{V-X} . Furthermore, finite-temperature magnetic transitions were systematically investigated through atomistic Monte Carlo simulations, which reveal that the sequence of Curie temperatures among different compositions and lattice types is primarily determined by J_{V-X} , with additional contributions from J_{X-X} exchange interactions. Importantly, we find that the V- X -V triangular pathway

framework remains valid even in partially-ordered systems from $L2_1$ to XA -type structures. Building on this insight, we propose the concept of “magnetic genes”, defined as the V- X -V triangular motif connected by NN exchange interactions J_{V-X} . We recognize that the magnetic genes could provide a promising concept for exploring the magnetic properties in more Heusler alloys.

II. METHODS

To perform the structural relaxation calculations, we use the VASP code [32, 33], which implements the projector-augmented wave (PAW) method [34] and is based on the GGA-PBE generalized gradient approximation [35]. A dense k -mesh of $10 \times 10 \times 10$ is employed for the structural relaxation calculations. The plane-wave cutoff was chosen to be 425 eV. The convergence criteria for the total energy and ionic forces were set to 10^{-7} eV and 10^{-3} eV/Å, respectively.

Additionally, we performed spin-polarized density-functional [36, 37] calculations using the ATOMIC-ORBITAL BASED AB-INITIO COMPUTATION AT USTC (ABACUS) package [38, 39], an open-source first-principles platform with advanced ground- and excited-state modules, and interfaces to Wannier90. We employed the SG15 optimized norm-conserving Vanderbilt (ONCV) pseudopotentials [40] and the same exchange correlation [35]. The Kohn-Sham wave functions were expanded using a linear combination of atomic orbitals corresponding to the SG15 ONCV (Version 2.0 standard orbitals) [39]. After convergence tests, the grid cutoff for numerical integrations was set to 100 Ry.

To explore the magnetic properties in V_2XAl , we employed the TB2J package [41], which is based on the use of Green’s functions. The real-space Heisenberg exchange parameters

$$J_{ij} = \frac{1}{4\pi} \int_{-\infty}^{E_F} dE \text{ImTr}[\Delta_i G_{ij}^{\uparrow}(E) \Delta_j G_{ji}^{\downarrow}(E)],$$

where Δ_i is the on-site exchange splitting and $G_{ij}^{\sigma}(E)$ the spin-resolved Green function. The complete set $\{J_{ij}\}$ defines a classical Heisenberg Hamiltonian

$$\mathcal{H} = - \sum_{i \neq j} J_{ij} \mathbf{S}_i \cdot \mathbf{S}_j,$$

which was solved with the VAMPIRE atomistic spin-dynamics code [42].

The simulated system of V_2XAl is a cubic box of edge length 15 nm, generated by replicating the relaxed face-centered unit cell and containing about 2.1×10^5 spins, which was evolved with a stochastic spin integrator. Temperatures from 0 to 1000 K in 5 K increments were sampled using 2.5×10^3 equilibration steps. The Curie temperature T_C was determined from the inflection point of the magnetization $M(T)$.

TABLE I. Spin magnetic moments m of each inequivalent atomic site and the total magnetic moment m_{tot} ($\mu_B/\text{f.u.}$) for V_2XAl ($X = \text{Cr, Mn, Fe, Co, Ni}$) compounds in the $L2_1$ -type structure, as obtained in this work and compared with previous literature [43].

Compound	$m_V(4b)$	$m_X(8c)$	$m_{Al}(4a)$	m_{tot}	Source
$L2_1$ - V_2CrAl	0.901	-0.742	0.026	1.085	This work
$L2_1$ - V_2MnAl	1.802	-2.018	0.068	1.653	This work
$L2_1$ - V_2MnAl	1.667	-1.653	-0.040	1.641	Jerzy <i>et al.</i> [43]
$L2_1$ - V_2FeAl	0.537	1.917	-0.021	2.970	This work
$L2_1$ - V_2FeAl	0.362	1.889	-0.014	2.599	Jerzy <i>et al.</i> [43]
$L2_1$ - V_2CoAl	1.238	1.136	0.024	3.636	This work
$L2_1$ - V_2NiAl	1.249	0.265	-0.005	2.757	This work

III. RESULTS AND DISCUSSION

A. Magnetic orders of fully-ordered $L2_1$ - and XA - V_2XAl

The magnetic ordering in Heusler alloys is strongly influenced by both their atomic composition and crystallographic structure. In this work, we focus on two prototypical lattice types, namely the $L2_1$ and XA structures. As established in previous studies, these two structural variants provide a well-defined platform for examining the role of chemical disorder without altering the overall structural topology [7, 14, 28]. As illustrated in Fig. 1(a), the $L2_1$ -type full-Heusler structure (space group $Fm\bar{3}m$, No.225) with the generic formula V_2XAl consists of V atoms occupying the $8c$ ($1/4, 1/4, 1/4$) Wyckoff positions, while Al and X atoms are located at the $4a$ ($0, 0, 0$) and $4b$ ($1/2, 1/2, 1/2$) sites, respectively [7]. By contrast, in the XA -type inverse-Heusler structure (space group $F\bar{4}3m$, No.216), shown in Fig. 1(b), the X atoms occupy the $4c$ ($1/4, 1/4, 1/4$) positions that arise from the symmetry breaking of the $8c$ sites in the $L2_1$ -type structure, while the V atoms are shifted to the $4b$ sites. From a broader perspective, the redistribution of atomic occupations between the $4c$ and $4b$ sites, driven by the evolution from $L2_1$ to XA -type structures, highlights the importance of chemical disorder in determining the magnetic properties of these compounds. A detailed analysis of disorder effects will be presented in Sec. III D.

We begin by examining the effect of atomic composition on the magnetic order in $L2_1$ -type V_2XAl ($X = \text{Cr, Mn, Fe, Co, Ni}$), where the crystal structure is relatively simple, containing only three inequivalent Wyckoff sites compared to the more complex XA -type structure. As summarized in Table I, compounds with $X = \text{Fe, Co, and Ni}$ exhibit ferromagnetic ordering, whereas those with $X = \text{Cr and Mn}$ display ferrimagnetic ordering characterized by antiparallel spin alignment between the X and V sublattices. In particular, our calculations show that V_2MnAl adopts a ferrimagnetic ground state, with magnetic moments of $+1.802 \mu_B$ per V atom and $-2.018 \mu_B$ per Mn atom. By contrast, V_2FeAl exhibits ferromagnetic ordering with a total magnetic moment of $2.970 \mu_B$

per formula unit, in agreement with previous reports [43]. Notably, the total magnetic moments of the $X = \text{Fe}$ to Ni compounds do not vary monotonically across the series. While the magnetic moments on the V sublattice increase progressively from Fe to Ni, those on the X site decrease rapidly, leading to non-monotonic behavior in the total moment. These complex magnetic orders and the non-monotonic variation in total magnetization are primarily attributed to differences in the underlying electronic structures arising from the atomic composition. A detailed discussion of the interplay between electronic structure and magnetic order will be presented in Sec. III E.

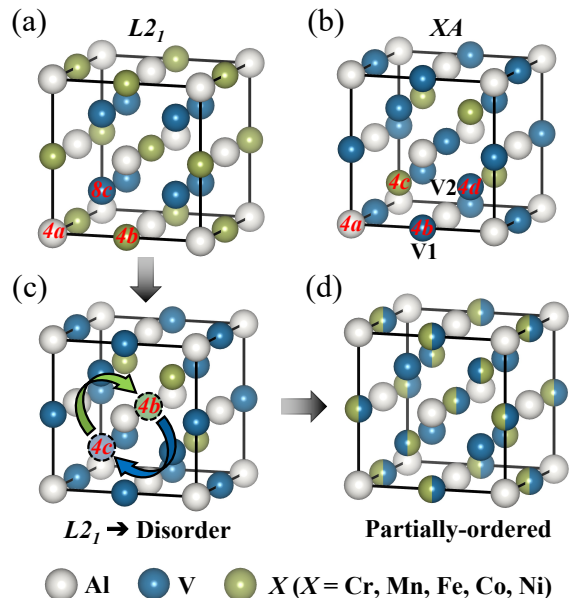


FIG. 1. Crystal structures of V_2XAl ($X = \text{Cr, Mn, Fe, Co, Ni}$) Heusler alloys. (a) Fully-ordered $L2_1$ -type full-Heusler ($Fm\bar{3}m$). (b) Fully-ordered XA -type inverse-Heusler ($F\bar{4}3m$). (c) Schematic pathway from $L2_1$ to XA through disorder. (d) Partially-ordered V_2XAl structure considered in this work.

TABLE II. Spin magnetic moments m of each inequivalent atomic site and the total magnetic moment m_{tot} ($\mu_B/\text{f.u.}$) for V_2XAl ($X = \text{Cr, Mn, Fe, Co, Ni}$) compounds in the XA -type inverse-Heusler structure. Results from this work are compared with previous studies.

Compound	$m_{V1}(4b)$	$m_{V2}(4d)$	$m_X(4c)$	$m_{Al}(4a)$	m_{tot}	Source
$XA-V_2CrAl$	-0.497	-1.397	1.774	-0.026	0.145	This work
$XA-V_2MnAl$	-0.820	1.466	1.610	0.007	2.264	This work
$XA-V_2MnAl$	-0.689	1.440	1.340	-0.082	2.009	Jerzy <i>et al.</i> [43]
$XA-V_2FeAl$	-0.447	2.043	1.179	0.002	2.777	This work
$XA-V_2FeAl$	-0.790	2.180	1.699	-0.120	2.950	Jerzy <i>et al.</i> [43]
$XA-V_2FeAl$	-0.310	2.110	1.20	0.090	3.090	Skaftouros <i>et al.</i> [31]
$XA-V_2CoAl$	-0.404	1.801	0.556	0.043	1.996	This work
$XA-V_2CoAl$	-0.54	2.16	0.50	-0.12	2.0	Zhang <i>et al.</i> [44]
$XA-V_2NiAl$	-0.526	1.527	0.107	0.039	1.148	This work
$XA-V_2NiAl$	-0.66	1.74	0.06	-0.06	1.08	Zhang <i>et al.</i> [44]

To investigate the influence of lattice type on magnetism, we next examine the XA -type inverse-Heusler V_2XAl compounds, which possess a more complex crystal structure with four inequivalent Wyckoff sites compared to the $L2_1$ -type structure. Interestingly, among these systems, only V_2CrAl exhibits ferromagnetic coupling between the two inequivalent V sites, while the magnetic moments at the V-4b and X-4c sites align antiferromagnetically, as summarized in Tables II. This contrasts sharply with the comparatively simple magnetic ordering observed in the $L2_1$ -type compounds. More specifically, apart from V_2CrAl , all other XA -type V_2XAl compounds ($X = \text{Mn, Fe, Co, Ni}$) display antiparallel alignment of the spin moments between the V atoms at the 4d and 4b sites. Our calculated magnetic moments for XA -type V_2XAl ($X = \text{Mn, Fe, Co}$) are in good agreement with previous reports [31, 43, 44]. Furthermore, the half-metallic compounds V_2MnAl and V_2FeAl exhibit total magnetic moments of 2.26 and 2.78 $\mu_B/\text{f.u.}$, respectively, which are close to the ideal values of 2 and 3 $\mu_B/\text{f.u.}$ predicted by the generalized Slater–Pauling relation of $M_{\text{tot}} \approx Z_t - 18$, where Z_t is the total valence-electron count [31, 45]. Notably, as X varies from Cr to Ni, the local magnetic moment of the X site decreases monotonically (from 1.77 to 0.11 μ_B), whereas the total moment evolves in a nonmonotonic manner. These results highlight the intricate and composition-dependent magnetic behaviors of inverse-Heusler V_2XAl compounds, motivating the need for a more general understanding of their underlying mechanisms.

B. Microscopic magnetic mechanism in $L2_1$ - and $XA-V_2XAl$

To gain deeper insight into the origin of magnetism in these systems, we investigate the magnetic exchange couplings (J) across different atomic compositions and lattice types. As discussed above, in the relatively simple $L2_1$ -type V_2XAl compounds, only those with $X =$

Cr and Mn exhibit ferrimagnetic order, characterized by anti-parallel spin alignment between the X and V atoms. Correspondingly, as shown in Figs. 2(a) and 2(b), the NN exchange coupling J_{V-Mn} (J_{V-Cr}) between Mn (Cr) atoms at the 4b site and V atoms at the 8c site is antiferromagnetic type, which has the largest value among all the other magnetic exchange couplings in these materials. In contrast, for $X = \text{Fe, Co, and Ni}$, the NN J_{V-X} coupling between the X and V atoms is ferromagnetic, as illustrated in Fig. 2(c). Meanwhile, the exchange interactions between X-X atoms are significantly weaker and do not play a decisive role in stabilizing the magnetic order. The V-V interactions, however, exhibit more intricate behavior. In V_2MnAl , both the NN and next-nearest-neighbor (NNN) V-V couplings, indicated by the gray line in Fig. 2(a), are ferromagnetic. However, the NN V-V coupling in V_2CrAl , colored by the gray line, acquires a finite antiferromagnetic contribution, as shown in Fig. 2(b). Taken together, these results indicate that antiferromagnetic V-Mn(Cr)-V exchange pathways form triangular motifs that ultimately stabilize ferromagnetic ordering among the V sublattice. Overall, our exchange-coupling analysis provides a microscopic explanation for the emergence of complex magnetic orders in $L2_1$ -type V_2XAl compounds.

Here, we investigate the physical mechanisms underlying the magnetic ordering in the more complex XA -type V_2XAl compounds. In these type compounds, the magnetic moments of V1 (4b site) and X (4c site) are aligned antiparallel, indicating dominant antiferromagnetic exchange coupling. As shown in Figs. 2(d) and 2(e), the NN exchange couplings J_{V1-X} (highlighted in blue) are strongly antiferromagnetic ($X = \text{Cr, Mn}$; couplings for $X = \text{Fe, Co, Ni}$ are omitted for clarity) and represent the primary factor stabilizing ferrimagnetic ordering between the X and V1 sublattices. In contrast, the NN exchange coupling J_{V2-X} between X and V2 (4d site), as shown in purple lines in Figs. 2(e) and 2(f), evolves rapidly from antiferromagnetic to ferromagnetic as X changes from Cr to Ni. This change of J_{V2-X} is consistent with the corre-

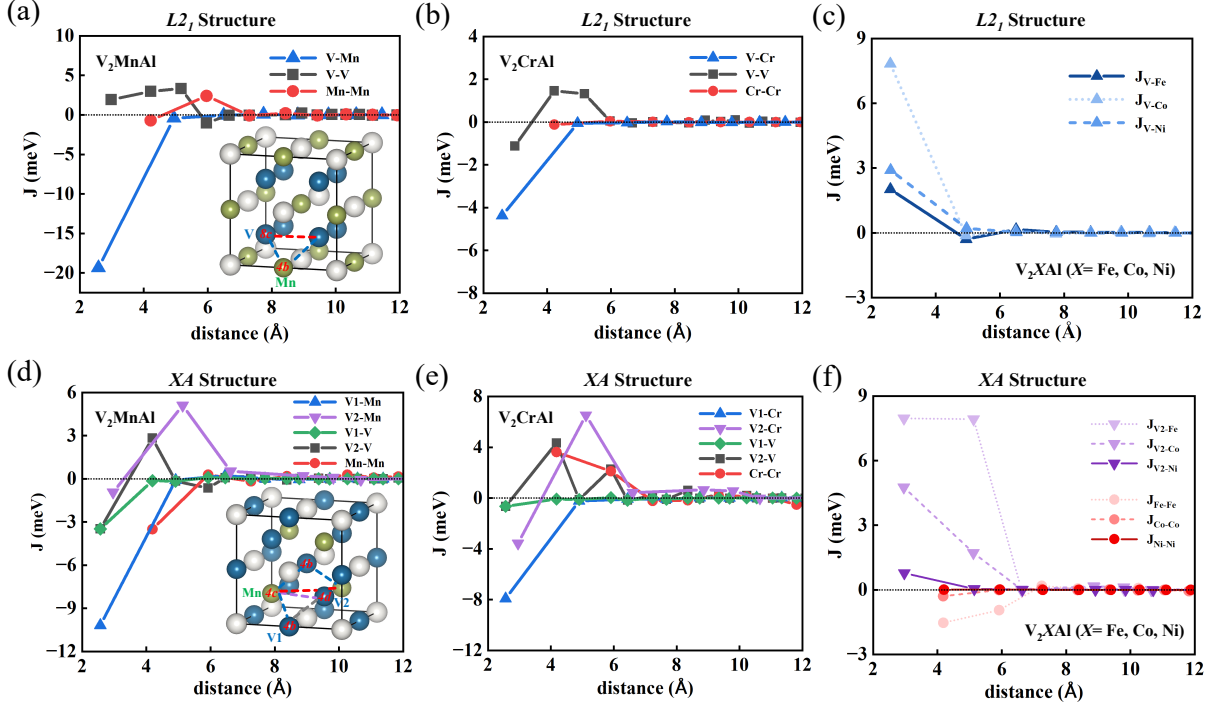


FIG. 2. Isotropic Heisenberg exchange parameters J for V_2XAl compounds. (a, b) J as a function of neighbor distance for $L2_1$ -type V_2MnAl and V_2CrAl , respectively. (c) NN exchange coupling J_{V-X} in $L2_1$ -type compounds with $X = Mn, Fe, Co, Ni$. (d, e) J as a function of neighbor distance for XA -type V_2MnAl and V_2CrAl , respectively. (f) NN exchange couplings J_{V2-X} and J_{X-X} in XA -type compounds with $X = Mn, Fe, Co, Ni$. Insets illustrate the triangular exchange pathways responsible for the observed magnetic orders.

sponding magnetic ordering from ferrimagnetic for $X = Cr$ to ferromagnetic for $X = Mn, Fe, Co$, and Ni . Notably, although the NN $V2-Mn$ interaction is weakly antiferromagnetic type, the NNN $V2-Mn$ coupling is strongly ferromagnetic, suggesting that V_2MnAl lies near a compositional boundary where the magnetic ordering transitions from ferrimagnetic to ferromagnetic with increasing X atomic number.

From our analysis of magnetic orders and exchange couplings, a comprehensive understanding of the overall magnetic behavior in V_2XAl across different atomic compositions and lattice types can be established. In $L2_1$ -type V_2XAl , the diverse magnetic orders can be rationalized in terms of triangular exchange pathways formed by $V-X-V$ atoms, as illustrated in the inset of Fig. 2(a). In XA -type V_2XAl , the underlying mechanism is similar, but an additional type of magnetic exchange coupling is present. Our results indicate that the $V1-X-V2$ triangular pathway remains a key determinant of magnetic order in XA -type compounds, as shown in the inset of Fig. 2(d). Changes in the type of the J_{V2-X} coupling substantially influence the magnetic ordering in these materials. Moreover, although the direct NN exchange coupling between $X-X$ atoms ($X = Mn, Fe, Co, Ni$) is antiferromagnetic type in $XA-V_2XAl$, the triangular $X-V1-X$ pathway ultimately stabilizes ferromagnetic

ordering due to the intervening antiferromagnetic $X-V1$ couplings, as illustrated in the inset of Fig. 2(d). In summary, despite variations in atomic composition and lattice type, the X site plays a central role in controlling the magnetic properties of V -based V_2XAl compounds through triangular pathways formed by NN V and X atoms. We therefore identify these motif as a candidate “magnetic genes”.

C. Magnetic transition temperature of $L2_1$ - and $XA-V_2XAl$

The microscopic mechanisms of magnetic exchange couplings directly determine the macroscopic magnetic properties. Based on our calculated exchange couplings in V_2XAl , we further simulate the magnetic transition temperatures across this series of Heusler compounds. As shown in Fig. 3(a), in $L2_1$ -type V_2XAl , V_2MnAl exhibits the highest Curie temperature, reaching approximately 900K, whereas the Curie temperatures of the remaining compounds ($X = Cr, Fe, Co, Ni$) are significantly lower, ranging from 100 K to 300 K. The exceptionally high Curie temperature of V_2MnAl originates from the effective ferromagnetic coupling between V atoms mediated by the triangular $V-Mn-V$ pathways, which

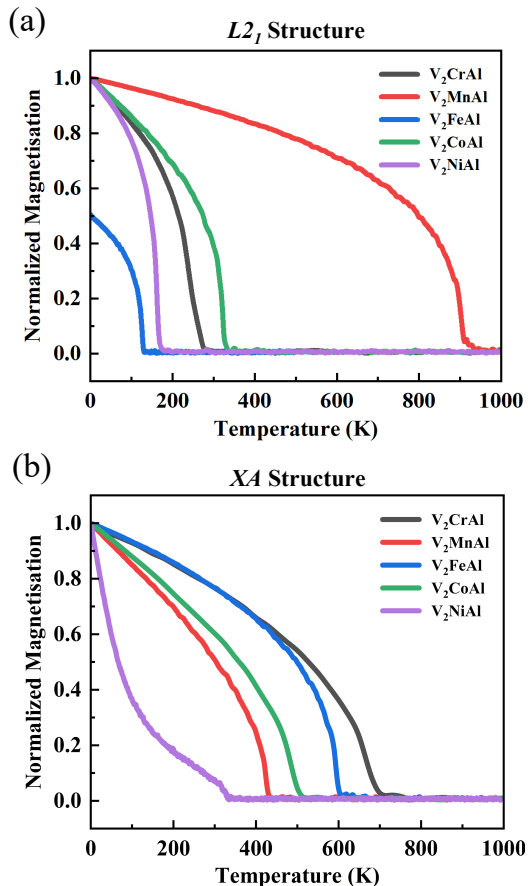


FIG. 3. (a) Temperature dependence of the normalized magnetic moments for V_2XAl compounds in $L2_1$ -type V_2XAl ($X = Cr, Mn, Fe, Co, Ni$). (b) Temperature dependence of the normalized magnetic moments for V_2XAl compounds in XA -type V_2XAl .

involve strong antiferromagnetic NN couplings J_{V-Mn} (~ -19.4 meV). This is further reinforced by the direct ferromagnetic V-V interactions. Remarkably, our Monte Carlo simulations reveal that the magnitude of the NN V-X exchange coupling J_{V-X} predominantly determines the magnetic transition temperature in $L2_1$ -type V_2XAl . Specifically, as shown in Fig. 3(a), T_C decreases from 900 K for V_2MnAl to 100 K for V_2FeAl , consistent with the corresponding NN exchange couplings J_{V-X} , which vary from -19.4 to 2.0 meV, as illustrated in Fig. 2.

The temperature dependence of magnetic phase transitions in XA -type V_2XAl compounds differs markedly from that in $L2_1$ -type structures. As shown in Fig. 3(b), the Curie temperatures in XA -type compounds vary within a narrower range, from approximately 700 K to 300 K, compared to the broader variation in $L2_1$ -type materials. This narrower range reflects the more complex network of magnetic exchange couplings in the inverse-Heusler structure. Specifically, V_2CrAl exhibits the high-

est T_C at about 700 K, while the Curie temperature gradually decreases as X changes from Fe to Ni. The magnetic transition temperature of V_2MnAl shows a slight anomaly, lying between the values for $X = Co$ and Ni . Despite the apparent complexity of these trends, they can be rationalized using the proposed microscopic mechanism based on the triangular exchange pathways. As discussed above, the NN exchange coupling J_{V-X} involving the X-site dominates the magnetic transition behavior. For instance, the relatively large J_{V1-Cr} contributes to the higher T_C in V_2CrAl . Although J_{V1-Mn} is also sizable, the T_C of V_2MnAl is significantly lower due to the additional influence of the J_{X-X} coupling. In V_2CrAl , the ferromagnetic $X-X$ interactions enhance T_C , whereas in V_2MnAl , the J_{X-X} coupling is antiferromagnetic, leading to a notable reduction of T_C . In the series $X = Fe, Co, Ni$, the gradual decrease of T_C is primarily driven by the weakening of the NN J_{V1-X} coupling, which diminishes from -3 to 0 meV.

In summary, the magnetic ground states and magnetic transition temperatures of V_2XAl compounds can be rationalized within the framework of the V-X-V triangular exchange pathway and its associated NN magnetic exchange couplings, applicable to both $L2_1$ - and XA -type structures. For simplicity, the NN exchange coupling J_{V-X} primarily governs the magnetic ordering, whereas the combination of J_{V-X} and J_{X-X} predominantly determines the magnetic transition temperature T_C . Although T_C depends on both the exchange couplings and the local magnetic moments of the constituent atoms, no straightforward correlation between the magnitude of individual magnetic moments and T_C is evident. Nevertheless, the observed trends in the dominant exchange couplings provide a practical framework to anticipate and potentially tune the Curie temperatures in these Heusler alloys.

D. Effect of chemical disorder on magnetism of partially-ordered V_2XAl

In V_2XAl compounds, the NN magnetic exchange coupling J_{V-X} plays a central role in determining both the magnetic ground states and the magnetic transition temperatures. This raises the question of whether this framework remains valid in the presence of chemical disorder. In this section, we investigate the evolution of magnetic order and magnetic transition temperatures under partial chemical disorder, introduced by progressively transforming the $L2_1$ -type structure toward the XA -type structure, as illustrated in Fig. 1(c) and 1(d). The introduction of disorder significantly reduces crystal symmetry, complicating the analysis of magnetic interactions. For clarity, we focus on the $L2_1$ -type V_2MnAl , which exhibits the highest Curie temperature among its sister compounds. Notably, our calculations show that the magnetic ground states remain robust across different degrees of chemical disorder. As summarized in Tables III,

TABLE III. Spin magnetic moments m of each inequivalent element and the total magnetic moment m_{tot} ($\mu_B/\text{f.u.}$) for partially-ordered V_2MnAl alloys considered in this work.

Structural ordering	m_{Mn}		m_{V_1}		m_{V_2}	m_{Al}	m_{tot}
	(4b)	(4c)	(4b)	(4c)	(4d)	(4a)	f.u.
100% $L2_1$	-2.018	—	—	1.802	1.802	0.068	1.653
75% $L2_1$ /25% XA	-1.863	2.936	-0.872	1.184	1.432	0.033	1.472
50% $L2_1$ /50% XA	-1.976	2.731	-0.926	0.630	1.474	0.016	1.719
25% $L2_1$ /75% XA	-1.593	1.582	-0.595	0.111	1.338	0.028	1.679
100% XA	—	1.610	-0.820	—	1.466	0.007	2.264

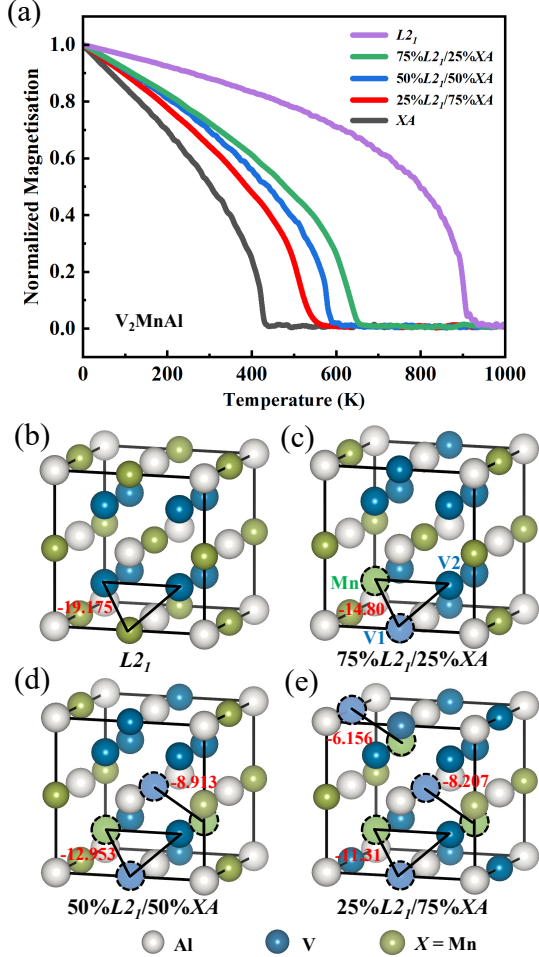


FIG. 4. (a) Temperature dependence of the normalized magnetic moment in partially-ordered V_2MnAl . (b-e) NN magnetic exchange couplings J_{V-X} for (b) fully-ordered $L2_1$, (c) 75% $L2_1$, (d) 50% $L2_1$, and (e) 25% $L2_1$ partially-ordered structures.

starting from the fully-ordered $L2_1$ -type structure, sequential swapping of Mn atoms in the 4b sites with V atoms in the 8c sites results in only minor reductions in the magnetic moment of V2 (nominal 4d site), which then stabilizes as the structure approaches the XA -type

configuration. Furthermore, despite atom swapping, the spin orientations at the corresponding Wyckoff sites are preserved. The magnetic moments of V atoms on both 4c and 4d sites decrease gradually from the $L2_1$ to the XA -type structure, as do the magnetic moments of Mn atoms on their respective sites. Overall, these results indicate that the intricate network of magnetic exchange couplings in V_2XAl is sufficiently robust to stabilize magnetic order even in the presence of substantial chemical disorder.

The magnetic transition temperature in partially-ordered V_2MnAl gradually decreases as the structure evolves from $L2_1$ to XA -type structure. As shown in Fig. 4(a), the Curie temperature T_C decreases from 900 K in the fully-ordered $L2_1$ structure to 420 K in the XA configuration. Within our framework, the NN magnetic exchange couplings J_{V-X} and J_{X-X} are the primary factors governing the magnetic transition temperature. In the partially-ordered structures studied here, swapping V and X atoms directly affects the NN coupling J_{V1-X} , while other magnetic exchange couplings are also modified. A comparison between the calculated Curie temperatures and the corresponding J_{V1-X} values in Fig. 4 shows a clear correlation. The magnitude of J_{V1-X} on the swapped sites closely tracks the variation of T_C . For instance, in 75% $L2_1$ - V_2MnAl , $J_{V1-\text{Mn}}$ is reduced to -14.8 meV, and further decreases to -11.3 meV (-8.2 meV and -6.1 meV for the other two relevant X sites) in 25% $L2_1$ - V_2MnAl , compared to -19 meV in the fully-ordered $L2_1$ structure. The rapid reduction of $J_{V1-\text{Mn}}$ from $L2_1$ to 75% $L2_1$ is reflected in the corresponding decrease of T_C from 990 K to 650 K.

Interestingly, within the V_2XAl series, the trend of magnetic transition temperatures in V_2FeAl is opposite to that observed in V_2MnAl . As shown in Fig. 5(a), the Curie temperature T_C of V_2FeAl gradually decreases from 600 K to 120 K as the structure evolves from XA -to $L2_1$ type. This observation raises the question of which factors primarily govern this anomalous sequence of magnetic transition temperatures. As discussed above, the NN magnetic exchange coupling between V1 and X (J_{V1-X}) plays a dominant role in determining T_C . Our calculations indicate that, although the sequence of T_C with increasing chemical order in V_2FeAl is reversed relative to V_2MnAl , the NN coupling J_{V1-X} remains a

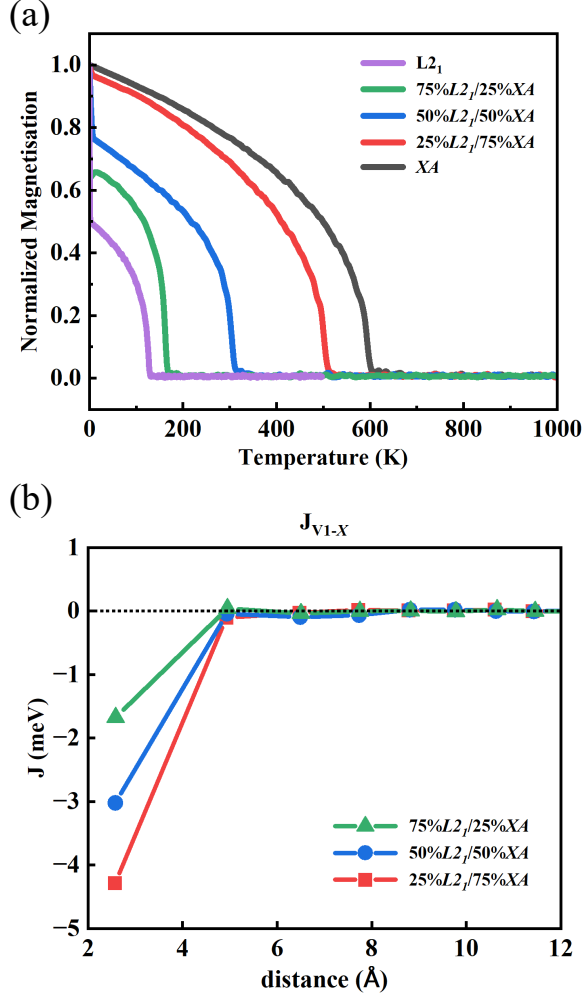


FIG. 5. (a) Temperature-dependent normalized magnetic moments for partially-ordered V_2FeAl alloys. (b) Nearest-neighbor magnetic exchange couplings J_{V1-X} for the corresponding partially-ordered V_2FeAl structures.

key factor. As shown in Fig. 5(b), the absolute value of J_{V1-X} decreases systematically from the XA - to the $L2_1$ -type structure, consistent with the observed reduction in T_C . These results confirm the validity of J_{V1-X} as the primary determinant of the Curie temperature in partially-ordered V_2FeAl .

Our calculations on partially chemically disordered V_2XAl indicate that the NN magnetic exchange coupling J_{V1-X} remains the dominant factor governing the magnetic transition temperature. Notably, during the transition from the $L2_1$ to the XA -type structure, the $4d$ site is consistently occupied by V2 atoms, ensuring that the V-X-V magnetic triangular pathway is preserved. Consequently, the microscopic magnetic mechanism in chemically disordered V_2XAl is still primarily governed by the V-X-V triangular pathway and the associated NN magnetic exchange couplings J_{V-X} .

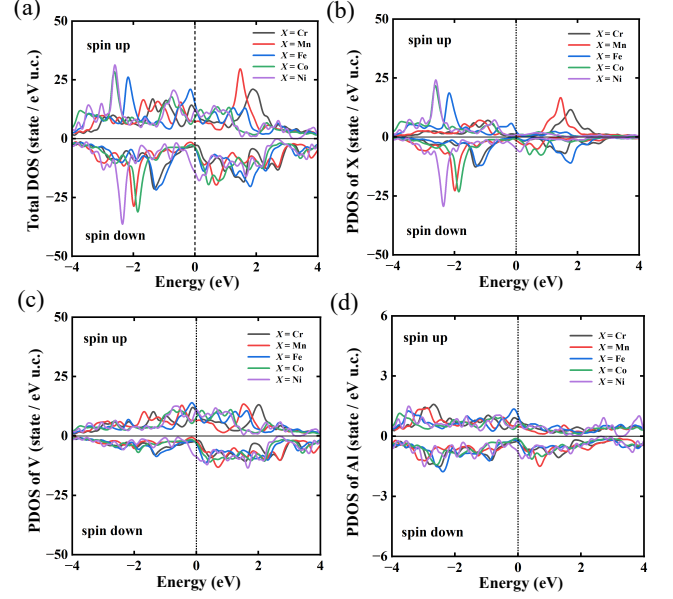


FIG. 6. (a) Total density of states for $L2_1$ -type V_2XAl ($X = Cr, Mn, Fe, Co, Ni$). (b) Partial DOS projected onto the X atoms in $L2_1$ -type V_2XAl . (c) Partial DOS projected onto the V atoms in $L2_1$ -type V_2XAl . (d) Partial DOS projected onto the Al atoms in $L2_1$ -type V_2XAl .

E. Electronic structures of fully-ordered V_2XAl

Based on the calculated magnetic ground states of $L2_1$ -type V_2XAl in Sec. III A, the observed complex magnetic orders and non-monotonic variation of total magnetic moments with atomic composition are proposed related to their electronic structures. In $L2_1$ -type V_2XAl , the relatively small total magnetic moments of V_2CrAl and V_2MnAl originate from the anti-parallel alignment of spin moments between the V and X sublattices. This behavior is clearly reflected in the calculated density of states (DOS). As shown in Fig. 6(a), the total DOS of $L2_1$ -type V_2XAl exhibits a high value at the Fermi level, indicating itinerant magnetism in these compounds [46–48]. Notably, several compounds display nearly half-metallic character. As shown in Fig. 6(b), Cr and Mn atoms exhibit pronounced occupied states with sharp peaks at approximately -1 eV and -2 eV in the spin-down channel, while their spin-up channel states are minimally occupied. In contrast, for $X = Fe, Co$, and Ni , the PDOS of X atoms shows significant occupation in the spin-up channel and comparatively low values in the spin-down channel. These electronic features are consistent with the observed transition in magnetic order from ferrimagnetism ($X = Cr, Mn$) to ferromagnetism ($X = Fe, Co, Ni$).

Furthermore, from $X = Fe$ to Ni , the PDOS of X atoms shifts to lower energies in both spin-up and spin-down channels, as shown in Fig. 6(b). This trend is at-

tributed to the increasing number of valence electrons with rising atomic number. The pronounced difference between the spin-up and spin-down PDOS of Fe atoms indicates a large magnetic moment on Fe in V_2FeAl , whereas the PDOS of Ni atoms in V_2NiAl is nearly symmetric between spin channels, reflecting a significantly reduced magnetic moment. Examination of the V-atom PDOS from $X = Fe$ to Ni reveals an increase in spin-up states below the Fermi level for V atoms in Co- and Ni-containing compounds, particularly in the energy range from -1 to 0 eV, as shown in Fig. 6(c), while the spin-down PDOS decreases in the same energy range. This behavior correlates with the observed increase in magnetic moments of V atoms from $X = Fe$ to Ni. In contrast, the PDOS of Al atoms remains largely unchanged across the series in Fig. 6(d), consistent with the negligible magnetic moment on Al atoms. Taken together, the change in magnetic order from $X = Mn$ to Fe, combined with the opposing trends in magnetic moments of V and X atoms from $X = Fe$ to Ni, accounts for the non-monotonic variation in the total magnetic moment across the V_2XAl series.

IV. CONCLUSION

In this work, we employed density functional theory calculations combined with Monte Carlo simulations based on Heisenberg magnetic exchange couplings to investigate V_2XAl alloys and introduced the concept of “magnetic genes”. These magnetic genes govern both

the magnetic ground states and the magnetic transition temperatures in fully- and partially-ordered compounds. The underlying physical mechanism arises from the modulation of NN magnetic exchange couplings J_{V-X} within the V-X-V triangular pathways, which is influenced by atomic composition, crystal structure, and the degree of chemical disorder. Using the framework of magnetic genes, the magnetic orders can be rationalized in terms of the V-X-V triangular pathways formed by NN J_{V-X} couplings. Furthermore, the magnetic transition temperatures are predominantly determined by both NN J_{V-X} and additional J_{X-X} magnetic exchange interactions, irrespective of whether the alloy is fully or partially ordered. We anticipate that the identification of magnetic genes in other Heusler alloys may provide a systematic and predictive approach to understanding and tuning their diverse magnetic properties.

ACKNOWLEDGMENTS

This work is supported by the National Natural Science Foundation of China (Grants No. 52371174 and No. 12204033), the Fundamental Research Funds for the Central Universities (Grant No. FRF-TP-22-097A1), the State Key Lab of Advanced Metals and Materials (Grant No. 2022Z-13), the Young Elite Scientist Sponsorship Program by BAST (Grant No. BYESS2023301) and the High-performance Computing Platform of University of Science and Technology Beijing.

-
- [1] S. Gupta, S. Chakraborty, V. Bhasin, S. Pakhira, S. Dan, C. Barreateau, J.-C. Crivello, S. N. Jha, M. Avdeev, J.-M. Greneche, D. Bhattacharyya, E. Alleno, and C. Mazumdar, High spin polarization in the disordered quaternary heusler alloy $femnvga$, *Phys. Rev. B* **108**, 045137 (2023).
 - [2] Y. Venkateswara, J. Nag, S. S. Samatham, A. K. Patel, P. D. Babu, M. R. Varma, J. Nayak, K. G. Suresh, and A. Alam, $FeRhCrSi$: Spin semimetal with spin-valve behavior at room temperature, *Phys. Rev. B* **107**, L100401 (2023).
 - [3] S. Nishihaya, M. J. A. Jardine, H. S. Inbar, A. Goswami, J. T. Dong, A. N. Engel, Y.-H. Chang, C. P. Dempsey, M. Hashimoto, D. Lu, N. Marom, and C. J. Palmström, Near-half-metallic state in the half-Heusler $PtMnSb$ film on a III-V substrate, *Phys. Rev. Mater.* **9**, 044403 (2025).
 - [4] R. A. de Groot, F. M. Mueller, P. G. v. Engen, and K. H. J. Buschow, New class of materials: Half-metallic ferromagnets, *Phys. Rev. Lett.* **50**, 2024 (1983).
 - [5] I. Žutić, J. Fabian, and S. Das Sarma, Spintronics: Fundamentals and applications, *Rev. Mod. Phys.* **76**, 323 (2004).
 - [6] M. I. Katsnelson, V. Y. Irkhin, L. Chioncel, A. I. Liechtenstein, and R. A. de Groot, Half-metallic ferromagnets: From band structure to many-body effects, *Rev. Mod. Phys.* **80**, 315 (2008).
 - [7] T. Graf, C. Felser, and S. S. Parkin, Simple rules for the understanding of Heusler compounds, *Progress in Solid State Chemistry* **39**, 1 (2011).
 - [8] A. Husmann and L. J. Singh, Temperature dependence of the anomalous hall conductivity in the Heusler alloy Co_2CrAl , *Phys. Rev. B* **73**, 172417 (2006).
 - [9] I. Shigeta, Y. Fujimoto, R. Ooka, Y. Nishisako, M. Tsujikawa, R. Y. Umetsu, A. Nomura, K. Yubuta, Y. Miura, T. Kanomata, M. Shirai, J. Gouchi, Y. Uwatoko, and M. Hiroi, Pressure effect on the magnetic properties of the half-metallic Heusler alloy Co_2TiSn , *Phys. Rev. B* **97**, 104414 (2018).
 - [10] J. Kübler, G. H. Fecher, and C. Felser, Understanding the trend in the curie temperatures of Co_2 -based Heusler compounds: Ab initio calculations, *Phys. Rev. B* **76**, 024414 (2007).
 - [11] N. M. Fortunato, X. Li, S. Schönecker, R. Xie, A. Taubel, F. Scheibel, I. Opahle, O. Gutfleisch, and H. Zhang, High-throughput screening of all- d -metal Heusler alloys for magnetocaloric applications, *Chemistry of Materials* **36**, 6765 (2024).
 - [12] M. Marathe and H. C. Herper, Exploration of all- $3d$ Heusler alloys for permanent magnets: An ab initio based high-throughput study, *Phys. Rev. B* **107**, 174402 (2023).

- [13] Y. Guo, C. Guo, Y. Xu, B. Zheng, X. Ni, and F. Tian, Machine learning investigation of chemical disorder effects in 24-valence-electron full-Heusler alloys with single magnetic element, *Journal of Magnetism and Magnetic Materials* **629**, 173322 (2025).
- [14] S. Picozzi, A. Continenza, and A. J. Freeman, Role of structural defects on the half-metallic character of Co_2MnGe and Co_2MnSi Heusler alloys, *Phys. Rev. B* **69**, 094423 (2004).
- [15] P. Devi, S. Singh, B. Dutta, K. Manna, S. W. D'Souza, Y. Ikeda, E. Suard, V. Petricek, P. Simon, P. Werner, S. Chadhov, S. S. P. Parkin, C. Felser, and D. Pandey, Adaptive modulation in the $\text{Ni}_2\text{Mn}_{1.4}\text{In}_{0.6}$ magnetic shape-memory Heusler alloy, *Phys. Rev. B* **97**, 224102 (2018).
- [16] T. Kanomata, Y. Chieda, K. Endo, H. Okada, M. Nagasako, K. Kobayashi, R. Kainuma, R. Y. Umetsu, H. Takahashi, Y. Furutani, H. Nishihara, K. Abe, Y. Miura, and M. Shirai, Magnetic properties of the half-metallic Heusler alloys Co_2VAl and Co_2VGa under pressure, *Phys. Rev. B* **82**, 144415 (2010).
- [17] H. Suto, V. Barwal, K. Simalaotao, Z. Li, K. Masuda, T. Sasaki, Y. Miura, and Y. Sakuraba, Negative spin polarization of Mn_2VGa Heusler alloy thin films studied in current-perpendicular-to-plane giant magnetoresistance devices, *Journal of Applied Physics* **135**, 203901 (2024).
- [18] S. Ouardi, G. H. Fecher, C. Felser, and J. Kübler, Realization of spin gapless semiconductors: The Heusler compound Mn_2CoAl , *Phys. Rev. Lett.* **110**, 100401 (2013).
- [19] O. Životský, K. Skotnicová, T. Čegan, J. Juřica, L. Gembalová, F. Zažímal, and I. Szurman, Structural and magnetic properties of inverse-Heusler Mn_2FeSi alloy powder prepared by ball milling, *Materials* **15**, 697 (2022).
- [20] S. Wurmehl, G. H. Fecher, H. C. Kandpal, V. Ksenofontov, C. Felser, H.-J. Lin, and J. Morais, Geometric, electronic, and magnetic structure of Co_2FeSi : Curie temperature and magnetic moment measurements and calculations, *Phys. Rev. B* **72**, 184434 (2005).
- [21] D. J. Singh and I. I. Mazin, Electronic structure, local moments, and transport in Fe_2VAl , *Phys. Rev. B* **57**, 14352 (1998).
- [22] S. Khmelevskiy, E. Simon, and L. Szunyogh, Antiferromagnetism in Ru_2MnZ ($Z = \text{Sn}, \text{Sb}, \text{Ge}, \text{Si}$) full Heusler alloys: Effects of magnetic frustration and chemical disorder, *Phys. Rev. B* **91**, 094432 (2015).
- [23] V. V. Sokolovskiy, V. D. Buchelnikov, M. A. Zagrebin, P. Entel, S. Sahoo, and M. Ogura, First-principles investigation of chemical and structural disorder in magnetic $\text{Ni}_2\text{Mn}_{1+x}\text{Sn}_{1-x}$ Heusler alloys, *Phys. Rev. B* **86**, 134418 (2012).
- [24] E. Decolvenaere, E. Levin, R. Seshadri, and A. Van der Ven, Modeling magnetic evolution and exchange hardening in disordered magnets: The example of $\text{Mn}_{1-x}\text{Fe}_x\text{Ru}_2\text{Sn}$ Heusler alloys, *Phys. Rev. Mater.* **3**, 104411 (2019).
- [25] T. Li, J. Duan, C. Yang, and X. Kou, Synthesis, microstructure and magnetic properties of Heusler Co_2FeSn nanoparticles, *Micro & Nano Letters* **8**, 143 (2013).
- [26] R. Smith, Z. Gercsi, R. Zhang, K. Siewierska, K. Rode, and J. Coey, Effects of disorder on the magnetic properties of the Heusler alloy V_2FeAl , *Acta Materialia* **267**, 119733 (2024).
- [27] O. N. Miroshkina, B. Eggert, J. Lill, B. Beckmann, D. Koch, M. Y. Hu, T. Lojewski, S. Rauls, F. Scheibel, A. Taubel, M. Šob, K. Ollefs, O. Gutfleisch, H. Wende, M. E. Gruner, and M. Friák, Impact of magnetic and antisite disorder on the vibrational densities of states in Ni_2MnSn Heusler alloys, *Phys. Rev. B* **106**, 214302 (2022).
- [28] I. Galanakis, P. H. Dederichs, and N. Papanikolaou, Slater-Pauling behavior and origin of the half-metallicity of the full-Heusler alloys, *Phys. Rev. B* **66**, 174429 (2002).
- [29] J. Chico, S. Keshavarz, Y. Kvashnin, M. Pereiro, I. Di Marco, C. Etz, O. Eriksson, A. Bergman, and L. Bergqvist, First-principles studies of the Gilbert damping and exchange interactions for half-metallic Heuslers alloys, *Phys. Rev. B* **93**, 214439 (2016).
- [30] F. Kuroda, T. Fukushima, and T. Oguchi, First-principles study of magnetism and phase stabilities of V2 based antiferromagnetic Heusler alloys, *Journal of Applied Physics* **127**, 193904 (2020).
- [31] S. Skaftouros, K. Özdoğan, E. Şaşıoğlu, and I. Galanakis, Generalized Slater-Pauling rule for the inverse Heusler compounds, *Phys. Rev. B* **87**, 024420 (2013).
- [32] G. Kresse and J. Furthmüller, Efficient iterative schemes for ab initio total-energy calculations using a plane-wave basis set, *Phys. Rev. B* **54**, 11169 (1996).
- [33] G. Kresse and D. Joubert, From ultrasoft pseudopotentials to the projector augmented-wave method, *Phys. Rev. B* **59**, 1758 (1999).
- [34] P. E. Blöchl, Projector augmented-wave method, *Phys. Rev. B* **50**, 17953 (1994).
- [35] J. P. Perdew, K. Burke, and M. Ernzerhof, Generalized gradient approximation made simple, *Phys. Rev. Lett.* **77**, 3865 (1996).
- [36] P. Hohenberg and W. Kohn, Inhomogeneous electron gas, *Phys. Rev.* **136**, B864 (1964).
- [37] W. Kohn and L. J. Sham, Self-consistent equations including exchange and correlation effects, *Phys. Rev.* **140**, A1133 (1965).
- [38] P. Li, X. Liu, M. Chen, P. Lin, X. Ren, L. Lin, C. Yang, and L. He, Large-scale ab initio simulations based on systematically improvable atomic basis, *Computational Materials Science* **112**, 503 (2016), computational Materials Science in China.
- [39] W. Zhou, D. Zheng, Q. Liu, D. Lu, Y. Liu, P. Lin, Y. Huang, X. Peng, J. J. Bao, C. Cai, Z. Jin, J. Wu, H. Zhang, G. Jin, Y. Ji, Z. Shen, X. Liu, L. Sun, Y. Cao, M. Sun, J. Liu, T. Chen, R. Liu, Y. Li, H. Han, X. Liang, T. Bao, N. Chen, H. Ren, X. Zhang, Z. Liu, Y. Fu, M. Liu, Z. Li, T. Wen, Z. Tang, Y. Xu, W. Duan, X. Wang, Q. Gu, F.-Z. Dai, Q. Zheng, J. Zhao, Y. Zhang, Q. Ou, H. Jiang, S. Liu, B. Xu, S. Xu, X. Ren, L. He, L. Zhang, and M. Chen, ABACUS: An electronic structure analysis package for the AI era, *arXiv e-prints*, 2501.08697 (2025).
- [40] M. Schlipf and F. Gygi, Optimization algorithm for the generation of ONCV pseudopotentials, *Computer Physics Communications* **196**, 36 (2015).
- [41] X. He, N. Helbig, M. J. Verstraete, and E. Bousquet, TB2J: A python package for computing magnetic interaction parameters, *Computer Physics Communications* **264**, 107938 (2021).
- [42] B. Skubic, J. Hellsvik, L. Nordström, and O. Eriksson, A method for atomistic spin dynamics simulations: imple-

- mentation and examples, *Journal of Physics: Condensed Matter* **20**, 315203 (2008).
- [43] J. Goraus, M. Fijałkowski, J. Czerniewski, and W. Gumulak, Magnetic properties of V_2MnGa , V_2MnAl , V_2FeGa and V_2FeAl , *Journal of Magnetism and Magnetic Materials* **585**, 171103 (2023).
- [44] X. Zhang, X. Dai, G. Chen, H. Liu, H. Luo, Y. Li, W. Wang, G. Wu, and G. Liu, First-principle study for full-Heusler compounds V_2YAl ($Y=V, Cr, Mn, Fe, Co, Ni$) and a discussion to Slater–Pauling rule, *Computational Materials Science* **59**, 1 (2012).
- [45] S. V. Faleev, Y. Ferrante, J. Jeong, M. G. Samant, B. Jones, and S. S. P. Parkin, Unified explanation of chemical ordering, the Slater–Pauling rule, and half-metallicity in full Heusler compounds, *Phys. Rev. B* **95**, 045140 (2017).
- [46] Y. Xu, Y.-C. Wang, X. Jin, H. Liu, Y. Liu, H. Song, and F. Tian, Mechanism of magnetic phase transition in correlated magnetic metal: insight into itinerant ferromagnet $Fe_{3-\delta}GeTe_2$, *Commun. Phys.* **7**, 381 (2024).
- [47] Y. Xu, X. Jin, J. Xiang, H. Zhang, and F. Tian, DFT + DMFT investigation of the magnetic phase transition in the itinerant ferromagnet Fe_3GaTe_2 , *Phys. Rev. B* **111**, 155142 (2025).
- [48] Y. Xu, X. Jin, H. Tang, and F. Tian, Electronic structures and magnetism in van der waals flat-band material Ni_3GeTe_2 , *Europhysics Letters* **151**, 36002 (2025).